Scientific Research Publishing

Journal of Applied Mathematics and Physics, 2022, 10, 1936-1950
https://www.scirp.org/journal/jamp
ISSN Online: 2327-4379
ISSN Print: 2327-4352

Fibonacci Stoichiometry and Superb Performance of $Nb_{16}W_5O_{55}$ and Related Super-Battery Materials

Hans Hermann Otto

Materialwissenschaftliche Kristallographie, Clausthal University of Technology, Clausthal-Zellerfeld, Lower Saxony, Germany
Email: hhermann.otto@web.de

How to cite this paper: Otto, H.H. (2022) Fibonacci Stoichiometry and Superb Performance of $Nb_{16}W_5O_{55}$ and Related Super-Battery Materials. *Journal of Applied Mathematics and Physics*, **10**, 1936-1950.
https://doi.org/10.4236/jamp.2022.106133

Received: May 17, 2022
Accepted: June 21, 2022
Published: June 24, 2022

Abstract

In this contribution, two important crystallographic concepts for the formation of a series of block structures associated with channeling have been compared: chemical twinning and crystallographic shear. Twin planes respectively shear planes besides formed channels serve as a sink for charge carriers or, when the oxidation state of metal ions can be reduced, as a reservoir for intercalated lithium. In this way, *Wadsley-Roth* shear phases such as niobium tungsten oxide $Nb_{16}^{5+}W_5^{6+}O_{55}$ exhibit channels for ultra-fast lithium-ion diffusion. They are in focus as anode material for super-batteries, superb in terms of energy respectively power density, charging time, cycle life and safety. It should be noted that the transition metal to oxygen ratio TM/O = 21/55 of the title compound is a *Fibonacci* number quotient. Also, the crystal lattice can be traced back to *Fibonacci* geometry. When replacing only 0.0213 tungsten atoms in the formula with less expensive titanium, a TM/O ratio of $0.381966 = \varphi^2$ can be adapted besides an average valence electron concentration of $2 \cdot \varphi^{-2}$, where $\varphi = \frac{\sqrt{5}-1}{2} = 0.6180339887$ represents the most irrational number of the golden mean. The additional disorder caused by even such small titanium replacement and accompanied oxygen vacancies could fasten up the already high lithium diffusion further. Ultrasonic treatment may be applied besides thermal cycling to prepare phase-pure $Nb_{16}^{5+}W_5^{6+}O_{55}$ of the highest electrochemical performance. A replacement of oxygen by some fluorine atoms is an obvious synthesis possibility, but the higher binding energy expected between lithium and fluorine in contrast to oxygen may rather hinder than promote lithium diffusion.

Keywords

Super Battery, Niobium Tungsten Oxide, Crystallographic Shear,

Chemical Twinning, Fibonacci Stoichiometry, Ti Substitution

1. Introduction

In the last years, excellent research was done to overcome the uneconomically long charging times and other odds of lithium-ion batteries, caused by the low performance of lithium intercalated graphite anodes. The best performance was now reached with the new anode material $Nb_{16}^{5+}W_5^{6+}O_{55}$ that can uptake more than 8 lithium ions per formula unit in its channel structure [1].

In the year 1965, two different mechanisms were described independently, by which homologous series of crystal structures can be formed. Chemical twinning was first described by *Otto* in the PbS-Bi_2S_3 binary system [2] [3] [4], and the crystallographic shear mechanism has been introduced by *Roth and Wadsley* [5]. The metal to anion ratio decreases in the case of chemical twinning, whereas in the case of crystallographic shear the ratio increases. We compare both systems of phase formation and their property to form channels near the twin planes respectively shear planes. These planes and channels can act as a sink for charge carriers or as housing for intercalated ions, if the metallic ions of the host lattice are able to undergo an alteration of the oxidation state. The top performance of the anode material $Nb_{16}^{5+}W_5^{6+}O_{55}$ with ultra-fast mobility of intercalated lithium ions may be coupled with a suggested disorder caused by its interesting transition metal to oxygen *Fibonacci* number ratio TM/O = 21/55. Super-ionic conduction depends on the "surface" defect density, which is evident since the work of *Lehovec* in 1953 [6] and is coupled to stoichiometry. We first highlight in Chapter 2 *the Fibonacci* number series and the golden mean, then compare chemical twinning in Chapter 3 with crystallographic shear in Chapter 4, and then perform a *Fibonacci* analysis of known niobium tungsten oxide shear phases, and finally suggest chemical alteration in Chapter 5. In addition, some examples were quoted, where *Fibonacci* nets are used by the present author to determine the position of heavy atoms in crystal structures.

2. Fibonacci Number Sequence and Golden Mean

As nature's effective-evolutionary pre-calculator, the golden ratio dominates all areas of science, life and cosmos. In physics, phase transitions are often governed by this number or its fifth power [7]. Stoichiometry as the numerical skeleton beyond chemistry should also not be excluded from a golden mean based explanation. So we begin with a short essay of number theory and the reciprocity property of this fundamental number and its connection with the *Fibonacci* number series [8]. The number series $F_n = \{0,1,1,2,3,5,8,13,21,34,55...\}$ was named after the *Italian* mathematician *Leonardo Pisano* named *Fibonacci* (1170-1240), where the sum of two succeeding numbers defines the next following number of the series: $F_n + F_{n+1} = F_{n+2}$ [7], while the quotient of F_n/F_{n+1}

for $n \to \infty$ determines the golden mean or golden ratio φ. The golden ratio is the most irrational number with the simplest infinite continued fraction representation at all and a very adaptable number-theoretical chameleon. Special attention is paid to the reciprocity property of the golden ratio as effective pre-calculator of natures creativness. We use the definition

$$\varphi = \frac{\sqrt{5}-1}{2} = \frac{1}{1+\dfrac{1}{1+\dfrac{1}{1+\cdots}}} = 0.6180339887\cdots \tag{1}$$

However, the golden ratio is frequently used by others as the reciprocal of this value

$$\varphi^{-1} = 1+\varphi = \frac{\sqrt{5}+1}{2} = 1.6180339887\cdots \tag{2}$$

Many examples for golden mean geometry are found in regular *Platonic* solids such as icosahedron or pentagonal dodecahedron [9], in the C_{60} bucky-ball [10] and in quasicrystals [11]. Also the structure of the elementary particle electron can be traced back to chiral icosahedral symmetry [12]. The stoichiometry of *Hume-Rothery* phases such as the Cu_5Zn_8 alloy indicates *Fibonacci* behavior with an average electron concentration equal to 21/13, fulfilling the *Hume-Rothery* electron concentration rule [13]. This leads directly to the explanations that follow. The golden ratio omnipresence in nature and life has been described in the highly recommended monograph by *Olsen* [14] and in the book "*Grand Unification of the Sciences*, *Arts and Consciousness*" by a well-known quartet of authors [15]. *Fibonacci* numbers in stoichiometry of chemical compounds have been also treated by *Vasyntinskij* [16].

3. Homologous Block Structures Formed by Chemical Twinning

The present author explained as first the mechanism of formation of block structures by chemical twinning [2] [3] [4]. Cationic vacancies, created by the substitution of Pb^{2+} by the smaller Bi^{3+} ion in the crystal structure of PbS (galena), are shown to be reduced by chemical twinning along the (311) twin plan. The first member of the series has the formula $6PbS{\cdot}Bi_2S_3$ and was found in nature as the mineral heyrovskyite. **Figure 1** shows its projected orthorhombic crystal structure with the typical PbS-like block structure, where Pb^{2+} on the twin plane has an increased sulfur coordination of 8 or 9 instead of 6. The crystallographic data are: space group *Bbmm* (No 63), a = 13.695 (3) Å, b = 31.358 (5) Å, c = 4.135 (1) Å, Z = 4, D_x = 7.29 $Mg{\cdot}m^{-3}$.

By reducing the block width one gets $3PbS{\cdot}Bi_2S_3$ composition (lillianite structure) [4]. As end member the $CaIrO_3$ structure type would result with Ca [8] and Ir [6] coordination. From this structure, the structure of Bi_2S_3 (bismuthinite) can be deduced by a distortion adapting sevenfold coordination for both Bi sites according to *Paulings* fifth crystal-chemical rule [17].

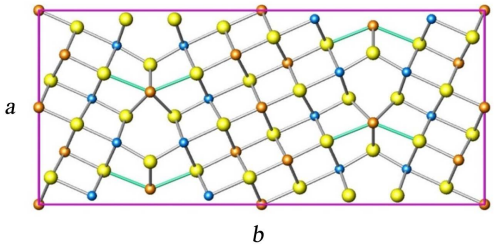

Figure 1. Projection of the orthorhombic crystal structure of $6PbS{\cdot}Bi_2S_3$ (heyrovskyite) down [001], exhibiting a galena-like block structure. Lead brownish, bismuth blue, sulfur yellow. Formed channels along [001] can be clearly seen on the vertical (311) twin plane at the height $b = ¼$.

4. The Wadsley-Roth Crystallographic Shear Phase $Nb_{16}^{5+}W_5^{6+}O_{55}$

In the Nb_2O_5-WO_3 binary system, *Roth and Wadsley* described a series of structures formed by crystallographic shear (see **Table 1**), exerted on the ReO_3 basis crystal structure (**Figure 2**), when the transition metal to oxygen ratio increases by replacement of some TM^{6+} by TM^{5+} or transition metal ions of even lower valence. In this way, anion vacancies are depleted, which have been enriched on certain planes, by edge-sharing of some oxygen octahedra. Crystallographic shear and shear propagation has been comprehensively described by *van Landuyt* [18].

The empty cage of the ReO_3 structure is surrounded by 12 oxygen atoms. In case of perovskites it is occypied by a large cation. Even in the perovskite $SrTiO_3$ crystallographic shear could be observed near dislocation [19].

Figure 3 shows the block of 4 by 5 ideal oxygen coordination octahedra and illustrates the 4-side windows, through which lithium ions can effectively jump.

The 4 by 5 octahedron extended single block structure of monoclinic $Nb_{16}^{5+}W_5^{6+}O_{55}$ as an example of shear structures has been displayed in **Figure 4** as projection down [010]. The crystallographic data are: monoclinic space group $C2$ (No 5), lattice parameters $a = 29.657$ (4) Å, $b = 3.8225$ (3) Å, $c = 23.106$ (4) Å, $ß = 126.50$ (1)˚, $Z = 2$, $D_x = 5.182$ Mg·m^{-3}. Because the block contains only 20 metal atoms, a supplementary W metal site is located at the shear plane boundaries at the cell origin respectively centering of the *ab*-plane. The process of lithianation causes only small lattice alterations. The lithium diffusion mechanisms have been investigated thoroughly by *Koçer et al.* and can be attributed to the entire family of *CS* phases [20]. Jumps between 4-sided windows have lowest activation energy and are considered as one-dimensional.

5. Proposal for Chemical Alterations and Preparation

We pose the question, whether the extreme super-ionic Li conduction of $Nb_{16}^{5+}W_5^{6+}O_{55}$ is (partly) caused by its *Fibonacci* number governed metal to oxygen ration of TM/O = 21/55 respectively the average valence electron concentration, and whether it is possible to further optimize the electrochemical

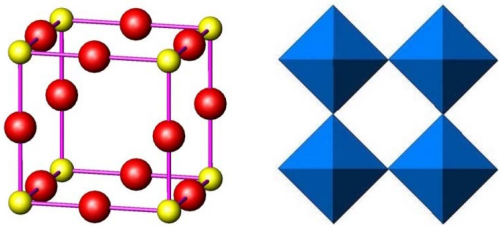

Figure 2. Prototypic crystal structure of cubic ReO_3, space group $Pm\bar{3}m$, a = 3.748 Å. Left: unit cell with yellow Re^{6+} and red O^{2-}. Right: projected corner-shared ReO_6 octahedra showing the large 4-sides window.

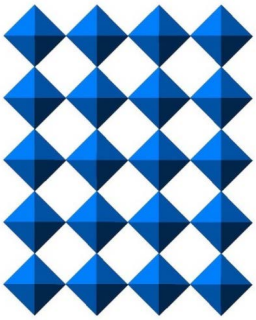

Figure 3. Checkerboard block of 4 by 5 ideal oxygen coordination octahedra around Re^{6+}. The block consists of 12 unit-cells. In the actual shear strucures, the outer octahedra are tilted slightly outwards to enable their edge linking to the next block.

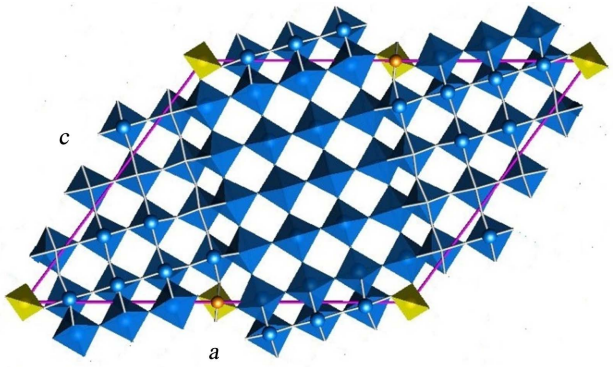

Figure 4. Crystal structure of $Nb_{16}W_5O_{55}$ projected down [010] [5]. Unit-cell magenta colored, tungsten yellow, niobium (tungsten) octahedra blue.

Table 1. *Fibonacci* anlysis of Nb_2O_5-WO_3 shear phases. In the proposed golden mean formulas the TM/O is adapted to φ^2 = 0.381966, whereas the average valence electron concentration $<c_{ve}>$ yields $2\cdot\varphi^{-2}$ = 5.236007.

Formula	Block Type	TM/O	$<c_{ve}>$	Golden Mean Formula
$Nb_{12}WO_{33}$	3 × 4	13/33 = 0.393939	5.077	$TM_{13}O_{34}$
$Nb_{14}W_3O_{44}$	4 × 4	34/88 = 0.386363	5.176	$TM_{34}O_{89}$
$Nb_{16}W_5O_{55}$	4 × 5	21/55 = 0.381818	5.231	$Nb_{16}W_{4.979}Ti_{0.0213}O_{54.979}$
$Nb_{18}W_8O_{69}$	5 × 5	13/34.5 = 0.37681	5.308	$Nb_{18}W_{7.07}Ti_{0.93}O_{68.07}$
$Nb_{18}W_{16}O_{93}$	5 × 5	34/93 = 0.365591	5.000	$Nb_{18}W_{12}Ti_4O_{89}$

performance by adapting a golden mean stoichiometry? For the TM/O ratio one finds

$$\frac{16+5}{55}=\frac{21}{55}=0.38181818\approx 0.3819660=\varphi^{2} \tag{3}$$

For the average valence electron concentration it yields

$$\frac{16\times 5+5\times 6}{16+5}=\frac{110}{21}=5.238095\approx 5.2360679=2\cdot\varphi^{-2} \tag{4}$$

Now we want to adapt exact golden mean values in the above relations by replacement of W^{6+} respectively Nb^{5+} by a small amount of Ti^{4+}. The wanted result is a replacement of only $\Delta=0.02128657Ti^{4+}$ for W^{6+} respectively $2\Delta=0.04257Ti^{4+}$ for Nb^{5+}, which is accompanied by an oxygen loss of Δ

$$\frac{21}{55-0.021286}=\varphi^{2} \tag{5}$$

$$\frac{110-0.04257}{21}=2\cdot\varphi^{-2} \tag{6}$$

Due to the very similar ionic radii of both W^{6+} and Ti^{4+} of r_{ion} = 0.42 Å a replacement seems to be possible in this limit. It can be suggested that the W site at the origin is affected. The crystal lattice would tolerate such a small replacement. However, a slightly altered cation to anion ratio towards M/O = 0.381966 = φ^2 could already be realized on the crystallite grain boundaries. But the question is, whether one could really expect any additional performance effect caused by such a small cationic replacement, introducing more disorder and some anion vacancies besides reducing stress for optimal lithium uptake? Only an experiment can verify it. With respect to very small differences in the free energy between adjacent phases of the Nb_2O_5-WO_3 binary system [21], it is recommended to try ultrasonic treatment besides thermal cycling during the preparation of nearly phase-pure samples of yellow-green $Nb_{16}^{5+}W_5^{6+}O_{55}$ nanomaterial. In this way an optimal electrochemical performance should be guaranteed. However, particle size and the architecture of the electrode with a large surface area are also important. Recently, J*ang* and *Zhao* proposed the fabrication of hollow nanotubes by electro-spinning methods [22].

6. Fibonacci Variation of the Shear Phase $Nb_{18}W_{16}O_{93}$

Another example is the shear phase $Nb_{18}W_{16}O_{93}$ [1] [21]. Again we can proceed as in Chapter 5 and replace W by Ti, but in an larger amount to propose the formula $Nb_{18}W_{12}Ti_4O_{89}$. Of course, the crystallographic data will change significantly compared to the starting phase. Nevertheless, a synthesis attempt could be interesting. For the TM/O ratio we found now

$$\frac{34}{89}=0.382022\approx\varphi^{2} \tag{7}$$

and for the average valence electron concentration

$$\frac{178}{34}=5.235294\approx 2\varphi^{-2} \tag{8}$$

Therewith we have applied the next higher *Fibonacci* number set. Again, a further little variation shifts the values in the exact golden mean power ratio.

$$\frac{34-0.005025}{89}=0.381966=\varphi^{2} \tag{9}$$

$$\frac{178}{34-0.005025}=5.2360679=2\varphi^{-2} \tag{10}$$

As an overall result we present in **Table 1** new golden mean-based formulas of crystallographic shear phases of the system Nb_2O_5–WO_6 for future synthesis routes to improve (by fortune) the electrochemical performance of battery materials. However, an initial TM/O ratio higher than $\varphi^2 = 0.381966$ means that additional oxygen would have to be accommodated in the lattice, and this should be ruled out.

The best adapted values to golden mean symmetry has $Nb_{16}^{5+}W_5^{6+}O_{55}$ and this phase should get our full attention. The phase $Nb_{18}W_8O_{69}$ [23] as oxygen reduced variant $Nb_{18}W_{7.07}Ti_{0.93}O_{68.07}$ is also interesting.

The *Fibonacci* analysis summarized in this **Table 1** indicates that consequent variation of $Nb_{18}W_{16}O_{93}$ would lead to a $Nb_{14}W_3O_{44}$ type phase. One could also add Nb_2O_5 as an end member of the niobium-tungsten-oxide homologous series with the *Fibonacci* number ratio TM/O = 2/5 = 0.4 > φ^2 to the table, but the crystal structure with fivefold coordinated polyhedra and without pronounced block formation behaves something differently to the tungsten-bearing compounds [24]. However, a colossal insulator-metal transition was recently observed in single-crystalline T-Nb_2O_5 films accessed by lithium [25] [26], where Li migration channels are oriented perpendicular to the film surface. Although the effect is different, it remembers the present author to the colossal conductance observed on oriented multiphase Y-Ba-Cu-O thin films [27] [28] [29], but also confirmed on a simple CuO-Cu interface [30] or on a $Ag_5Pb_2O_6$/CuO composite [31]. As the first researchers, we used at that time a (110) $SrTiO_3$ substrate for thin film deposition [27], now also used successfully for T-Nb_2O_5 deposition [25]. However, also a hexagonal graphene sheet could serve as substrate for T-Nb_2O_5 thin film deposition, when calculating between both surfaces the index of overall atomic distance deviation.

7. *Fibonacci* Nets Compared to Projected Shear Phase Lattices

The crystal structure of hexagonal $Bi_{6.3}JS_9$ served as example to develop the *Fibonacci* net concept [2] [32]. In **Figure 3** such a net and its mirror image is displayed showing 13 sub-cells. If the sub-cells would be decorated with heavy atoms, then the strongest *X*-ray diffraction intensities could be observed for reflections having *Miller* indices $31\bar{4}0$ and $52\bar{7}0$, giving index sums of $h^2 + k^2 + hk = 13$ respectively 3×13. The angle α between sub-cell direction and *a*-axis can be calculated as

$$\delta_{13} = \arctan\left(\frac{5}{3\sqrt{3}}\right) - 30 = 13.898^{\circ}. \quad (11)$$

Such net, helically twisted to a tubule, has been connected with tubulin microtubules that show strongest reinforcement of the ordered pattern when the protofilament number equals even $PF = 13$ [33]. Such dominant architecture may be also the basis for quantum computer architecture and can be shared with considerations regarding human consciousness [7].

On can proceed with a further hexagonal *Fibonacci* net having 21 sub-cells with strongest $41\bar{5}0$ lattice planes and the index sum of $4^2 + 1 + 4 = 21$, which is again a *Fibonacci* number.

The offset angle is calculated to be

$$\delta_{21} = \arctan\left(\frac{2}{\sqrt{3}}\right) - 30 = 10.893^{\circ}. \quad (12)$$

Coordinates of both nets are given in the **Appendix**. Although the lattices of niobium tungsten oxides deviate strongly from hexagonal symmetry, their monoclinic unit-cells with monoclinic angles near 120˚ show interesting similarities to the *Fibonacci* nets.

When comparing the simplest 3 by 4 block shear structure of $Nb_{12}WO_{33} = TM_{13}O_{33}$ (**Figure 5**) with the 13 sub-cell *Fibonacci* net, one can identify similar atomic arrangements, marked by red lines starting from the tungsten site at the "origin". In the 4 by 5 block structure of $Nb_{16}^{5+}W_5^{6+}O_{55}$ (**Figure 4**), one can identify details of a 21 sub-cell *Fibonacci* net (right side of **Figure 6**). We have to consider in the different crystal structures an atom at the "origin" and a block of atoms, giving $1 + 3 \times 4 = 13$ respectively $1 + 4 \times 5 = 21$, and $1 + 5 \times 5 = 2 \times 13$. However, we have two formula units each and therefore the double number of atoms. In **Figure 7** a crystallographic interpretation is given by comparing the metal sites with positions of a *Fibonacci* net, using a transformed unit-cell with exact 120˚ angle and lattice parameters of $a' = 2c'$ to adapt *C*-centering of the

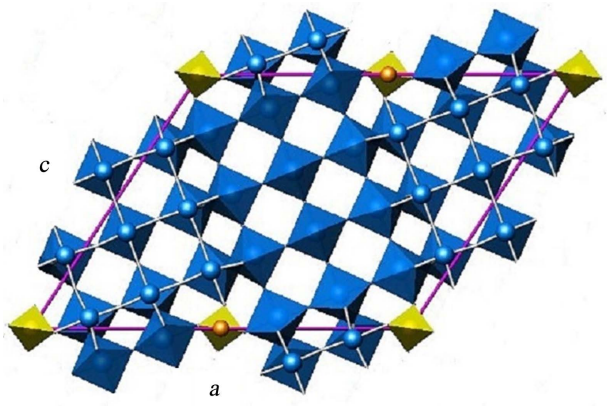

Figure 5. Crystal structure of $Nb_{12}WO_{33}$ projected down [010]. Space group *C*2, $a = 22.37$ Å, $b = 3.825$ Å, $c = 17.87$ Å, $\beta = 123.6^{\circ}$, $Z = 2$, $D_x = 4.76$ Mg·m^{-3} [5]. Tungsten (yellow tetrahedra, brownish sphere) joins four neighboring 3 × 4 blocks. The atomic arrangement highlighted by red lines can be compared with that on the *Fibonacci* net in **Figure 6**.

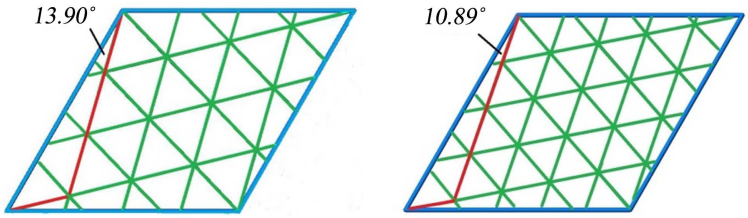

Figure 6. *Fibonacci* arrangement of hexagonal nets [2] [32] [34]. Unit-cells blue outlined, left: 13 sub-cells (green), offset by an angle of α = 13.9˚, right: 21 sub-cells, offset angle 10.9˚.

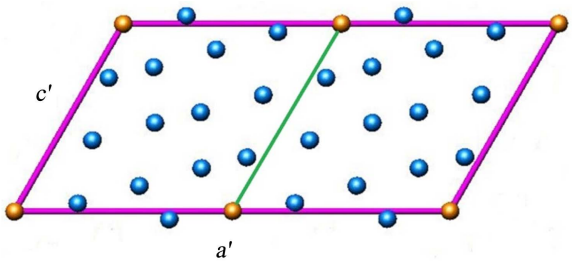

Figure 7. Transformed unit-cell of $Nb_{12}WO_{33}$ indicating a *Fibonacci*-like net of *TM* sites. In the left "hexagonal" half-cell, limited by the green line, exactly 13 transition metal sites can be identified.

original cell. Coordinates of the $Nb_{12}WO_{55}$ structure have been exemplarily compared with these of the 13 sub-cell *Fibonacci* net. In the middle part of **Figure 7**, representing the inner *TM* block and suffering not of atomic shifts by crystallographic shear, an almost hexagonal net is located. The sufficient agreement between both sets of coordinates suggests using such *Fibonacci* approach to crystal structure determination, because the phases of a large number of *X*-ray reflections are in this way correctly fixed (**Table A2**). The *Fibonacci* analysis suggests furthermore that strong reflections of the *X*-ray powder patterns of the shear phases should show a *Fibonacci* number indexing. Years ago, the present author has successfully applied *Fibonacci* lattice decoration with heavy atoms to determine crystal structures [32] [35]. A *Fibonacci* net with 21 sub-cells was used to determine the heavy atomic positions of zeolitic $Pb_6[Ge_6O_{18}]\cdot 2H_2O$ respectively of the crystal water free compound, space group $R\bar{3}$. From the hexagonal lattice parameter *a* we could find the positions of the sub-cell lattice with $a_{sub} = a/\sqrt{21}$ and offset angle $\delta_{21} = 60 - \arccos\left(\frac{3}{\sqrt{21}}\right) = 10.89^{\circ}$ (see also equation 12) [35].

8. Fluorination Synthesis Approach

A replacement of oxygen by some fluorine atoms is an obvious synthesis possibility, but the higher binding energy expected between lithium and fluorine in contrast to oxygen may rather hinder than promote lithium diffusion to obtain optimum performance. However, the example of lithium insertion in titanium oxyfluoride, $TiOF_2$, teaches us not to rule out such a synthesis route [36]. When

replacing for example maximum oxygen by fluorine in $Nb_{16}^{5+}W_{5}^{6+}O_{55}$ by maintaining the *Fibonacci* stoichiometry, one would get a tungsten-free hypothetical compound of formula $Nb_{11}^{5+}Ti_{10}^{4+}O_{40}F_{15}$ as a cheap alternative. The smaller radii of substituted ions would influence the channel diameters a little bit, assuming such a phase would exist.

9. The Mysterious Niobium

The special properties of niobium leading to many high-tech applications point towards a possible raw material competition situation in near future. This hardly fully understood metal with 5 electrons in its outer valence shells and oxidation states, ranging from −1 to +5, was in its history frequently in the focus of science. As pure metal it shows among all metals the highest superconducting transition of 9.25 K [37] and a transition of 23.2 K, when alloyed with germanium to A15-type Nb_3Ge [38] [39]. If one supposes that holes are essentially involved in the superconductivity of conventional materials as well [40] [41], especially niobium should be investigated in this direction anew. Niobium is also used as steel strengthener in super-alloys. Other interesting properties have been found in compounds of niobium such as pyrochlore, $(Na, Ca)_2Nb_2O_6(OH, F)$, which is the main niobium-bearing mineral raw material. The world's largest pyrochlore deposit, worked in the open pit, is located in Brazil near Araxá, Minas Gerais [42]. The carbonatitic complex contains bariopyrochlore with 16.5 wt% BaO and 63.5 wt% Nb_2O_5 [43] [44]. The pyrochlore structure, space group $Fd\bar{3}m$, shows as one of the simplest interacting systems (*Ising* ice model) frustrated magnetism and magnetic monopole formation [45].

Turning again to niobium tungsten oxides and their hidden properties, researchers look always at the oxidation states of niobium, but should also investigate the state of oxygen and conceivable holes located at oxygen, frequently being unobserved. The reader may study the work of *Gippius et al.* to get some ideas [46]. Catalytic properties of niobium oxides are due to the ability to dissociate hydrogen and its absorption in the crystal lattice [47]. Another aspect is the acentricity of the phases, which can significantly determine their physical properties. If we stay with *Fibonacci* number 13 again, the electron number of Nb^{2+} is 3×13. The chemistry of a compound is determined by the orchestra of electrons involved, but we have not yet dealt with the higher octaves.

10. Conclusion

Vacant atomic sites generated by chemical substitution in simple prototypic structures can be cut back by different mechanisms depending on whether they are cation vacancies or anion ones. Whereas cation vacancies can be removed by chemical twinning, anion vacancies can be cut back by crystallographic shear. Thereby structural channels will be generated allowing the intercalation of hydrogen respectively lithium and their super-ionic exchange as evidenced by the crystallographic shear phases of the Nb_2O_5-WO_3 system. From a *Fibonacci* stoi-

chiometry analysis, some suggestions for the alteration of chemistry and preparation of crystallographic shear phases of this system are derived with special attention to super-ionic $Nb_{16}^{5+}W_5^{6+}O_{55}$. These proposals include the replacement of a small amount of W^{6+} by Ti^{4+} to adapt exact golden mean stoichiometry to gain disorder and the highest electrochemical performance. The substitution would cause some oxygen vacancies, which could reduce stress and support lithium diffusion and mobility further. Phase-pure material may be synthesized by ultrasonic treatment besides thermal cycling. The complex disorder landscape of phases of the Nb_2O_5-WO_3 system may be understood rather well by a *Fibonacci* stoichiometry analysis besides *Fibonacci* lattice arguments. The secrets of nature can only be unraveled with a more holistic approach, bringing different aspects of one object together.

Conflicts of Interest

The author declares no conflict of interests regarding the publication of this paper.

References

[1] Griffith, K.J., Wiaderek, K.M., Cibin, G., Marbella, L.E. and Grey, C.P. (2018) Niobium Tungsten Oxides for High-Rate Lithium-Ion Energy Storage. *Nature*, **559**, 556-563. https://doi.org/10.1038/s41586-018-0347-0

[2] Otto, H.H. (1965) Zur Kristallchemie Synthetischer Blei-Wismut-Spießglanze. Diplom Thesis TU, Berlin, 1-65.

[3] Otto, H.H. und Strunz, H. (1967) Zur Kristallchemie Synthetischer Blei-Wismut-Spießglanze. 45. Jahrestagung der DMG, Berlin, 24-25.

[4] Otto, H.H. und Strunz, H. (1968) Zur Kristallchemie Synthetischer Blei-Wismut-Spießglanze. *Neues Jahrbuch für Mineralogie Abhandlungen*, **108**, 1-19.

[5] Roth, R.S. and Wadsley, A.D. (1965) Multiple Phase Formation in the Binary System Nb_2O_5-WO_3. II. The Structure of the Monoclinic Phases $WNb_{12}O_{33}$ and $W_5Nb_{16}O_{55}$. *Acta Crystallographica*, **19**, 32-38. https://doi.org/10.1107/S0365110X65002724

[6] Lehovec, K. (1953) Space-Charge Layer and Distribution of Lattice Defects at the Surface of Ionic Crystals. *Journal of Chemical Physics*, **21**, 1123-1128. https://doi.org/10.1063/1.1699148

[7] Otto, H.H. (2020) Phase Transitions Governed by the Fifth Power of the Golden Mean and Beyond. *World Journal of Condensed Matter Physics*, **10**, 135-158. https://doi.org/10.4236/wjcmp.2020.103009

[8] Pisano, L. (1202) Fibonacci's Liber Abaci (Book of Calculation). Biblioteca a Nazionale di Firenze, Florence.

[9] Otto, H.H. (2021) Ratio of In-Sphere Volume to Polyhedron Volume of the Great Pyramid Compared to Selected Convex Polyhedral Solids. *Journal of Applied Mathematics and Physics*, **9**, 41-56. https://doi.org/10.4236/jamp.2021.91005

[10] Kroto, H.W., Health, J.R., O'Brien, S.C., Curt, R.F. and Smailey, R.E. (1985) C_{60} Buckminsterfullerene. *Nature*, **318**, 162-163. https://doi.org/10.1038/318162a0

[11] Shechtman, D., Blech, I. Gratias, D. and Cahn, J. (1984) Metallic Phases with Long-Range Orientational Order and No Translational Symmetry. *Physical Review Letters*, **53**, 1951-1953. https://doi.org/10.1103/PhysRevLett.53.1951

[12] Otto, H.H. (2022) Golden Quartic Polynomial and Moebius Ball Electron. *Journal of Applied Mathematics and Physics*, **10**, accepted for publication. https://doi.org/10.4236/jamp.2022.105124

[13] Hume-Rothery, W. (1936) The Structure of Metals and Alloys. *Nature*, **138**, 7-8. https://doi.org/10.1038/138007a0

[14] Olsen, S. (2006) The Golden Section: Nature's Greatest Secret. *Bloomsbury*, 64 pp.

[15] Olsen, S., Marek-Crnjak, L., He, J.-H. and El Naschie, M.S. (2021) A Grand Unification of the Sciences, Arts & Consciousness. Scott Olsen, Ocala, 145 p.

[16] Vasyntinskij, N.A. (1989) Fibonacci Numbers in Stoichiometry of Chemical Compounds. *Izvestiya Akademii Nauk SSSR*, *Neorganicheskie Materialy*, **25**, 799-803.

[17] Otto, H.H. (2016) Didactics in Crystallography: The Crystal Structure of Bismuthinite, Bi_2S_3, Explained by Pauling's Fifth Crystallchemical Rule. Researchgate, 1-5.

[18] Van Landuyt, J. (1974) Shear Structures and Crystallographic Shear Propagation. *Journal de Physique Colloques*, **35**, C7-53-C7-63. https://doi.org/10.1051/jphyscol:1974704

[19] Du, H., Jia, C.-L. and Mayer, J. (2019) Local Crystallographic Shear Structure in [201] Extended Mixed Dislocations of $SrTiO_3$ Unraveled by Atomic-Scale Imaging Using Transmission Electron Microscopy and Spectroscopy. *Faraday Discussions*, **213**, 245-258. https://doi.org/10.1039/C8FD00102B

[20] Koçer, C.P., Griffith, K.J., Grey, C.P. and Morris, A.J. (2020) Lithium Diffusion in Niobium Tungsten Oxide Shear Structures. *Chemistry of Materials*, **32**, 3980-3989. https://doi.org/10.1021/acs.chemmater.0c00483

[21] Kerr, R.D. (2020) Synthesis and Characterization of Intergrowth Tungsten Bronzes and Evaluation of Their Electrochemical Performance. Durham E-Theses, Durham University, Durham, 1-71.

[22] Jang, J. and Zhao, J. (2021) Wadsley-Roth Crystallographic Shear Structure Niobium-Based Oxides: Promising Anode Material for High-Safety Lithium Ion Batteries. *Advanced Science*. https://doi.org/10.1002/advs.202004855

[23] Griffith, K. and Grey, C. (2020) Superionic Lithium Intercalation through 2nm x 2nm Colums in the Crystallographic Share Phase $Nb_{18}W_8O_{69}$. *Chemistry of Materials*, **32**, 3860-3868. https://doi.org/10.1021/acs.chemmater.9b05403

[24] Kato, K. and Tamura, S. (1975) Die Kristallstruktur von T-Nb_2O_5. *Acta Crystallographica*, **B31**, 673-677. https://doi.org/10.1107/S0567740875003603

[25] Han, H., Jacquet, Q., Jiang, Z., Sayed, F.N., Sharma, A., Schankler, A.M., Kakekhani, A., Meyerheim, H.L., Jeon, J.-C., Park, J., Nam, S.Y., Griffith, K.J., Simonelli, L., Rappe, A.M., Grey, C.P. and Parkin, S.S.P. (2022) Hidden Phases and Colossal Insulator-Metal Transition in Single-Crystalline T-Nb_2O_5 Thin Films Accessed by Lithium. arXiv:2203.03232 [cond-mat.mtrl-sci].

[26] Rani, R.A., Zoolfakar, A.S., O'Mallane, A.P., Austin, M.W. and Kalandar-Zadeh, K. (2014) Thin Films and Nanostructures of Niobium Pentoxide: Synthesis Methods and Applications. *Journal of Materials Chemistry A*, **2**, 15683-15703. https://doi.org/10.1039/C4TA02561J

[27] Schönberger, R., Otto, H.H., Brunner, B. and Renk. K. (1991) Evidence for Filamentary Superconductivity up to 220 K in Oriented Multiphase Superconducting Y-Ba-C-O Thin Films. *Physica C*, **171**, 159-162. https://doi.org/10.1016/0921-4534(91)90363-4

[28] Otto, H.H. (2016) High-T_c Superconductivity: Strong Indication of Filamentary-Chaotic Conductance and Possible Routes to Superconductivity above Room

Temperature. arXiv:1604.01623v1[physics.gen-ph].

[29] Otto, H.H. (2016) A Different Approach to High-T_c Superconductivity: Indication of Filamentary-Chaotic Conductance and Possible Routes to Superconductivity above Room Temperature. *World Journal of Condensed Matter Physics*, **6**, 244-260. https://doi.org/10.4236/wjcmp.2016.63023

[30] Osipov, V.V., Kochev, I.V. and Naumov, S.V. (2001) Electric Conductivity at the CuO-Cu Interface: HTSL-Like Temperature Variations. *Journal of Experimental and Theoretical Physics*, **93**, 1082-1092. https://doi.org/10.1134/1.1427119

[31] Djurek, D. (2011) $Ag_5Pb_2O_6$/CuO Composite, an Approach to Ambient Temperature Superconductivity. *Journal of Superconductivity and Novel Materials*, **24**, 199-203. https://doi.org/10.1007/s10948-010-0919-1

[32] Otto, H.H. (2015) Pyroelectric $Bi_{5-x}(Bi_2S_3)_{39}I_{12}S$: Fibonacci Superstructure, Synthesis Options and Solar Cell Potential. *World Journal of Condensed Matter Physics*, **5**, 66-77. https://doi.org/10.4236/wjcmp.2015.52010

[33] Wade, R.H., Chrétion, D. and Job, D. (1990) Characterization of Microtubule Protofilament Numbers. How Does the Surface Accomolate? *Journal of Molecular Biology*, **212**, 775-786. https://doi.org/10.1016/0022-2836(90)90236-F

[34] Otto, H.H. (2021) Beyond a Quartic Polynomial Modeling of the DNA Double-Helix Genetic Code. *Journal of Applied Mathematics and Physics*, **9**, 2558-2577. https://doi.org/10.4236/jamp.2021.910165

[35] Otto, H.H. and Brandt, H.J. (1996) $Pb_6(Ge_6O_{18}]\cdot 2H_2O$, a Lead Cyclo-Germanate Similar to the Mineral Dioptase. *European Journal of Mineralogy*, **8**, 301-310. https://doi.org/10.1127/ejm/8/2/0301

[36] Louvain, N., Karkar, Z., El-Ghozzi, M., Bonnet, P., Guérin, K. and Willmann, P. (2014) Fluorination of Anatase TiO_2 towards Titanium Oxyfluoride $TiOF_2$: A Novel Synthesis Approach and Proof of the Li-Insertion Mechanism. *Journal of Materials Chemistry*, **2**, 15308-15315. https://doi.org/10.1039/C4TA02553A

[37] Finnemore, D.K., Stromberg, T.F. and Swenson, C.A. (1966) Superconducting Properties of High-Purity Niobium. *Physical Review*, **149**, 231-243. https://doi.org/10.1103/PhysRev.149.231

[38] Matthias, B.T., Geballe, T.H., Willens, R.H., Corenzwit, E. and Hull Jr., G.W. (1973) Superconductivity of Nb_3Ge. *Physical Review*, **139**, A1501-A1503. https://doi.org/10.1103/PhysRev.139.A1501

[39] Cohn, R.J. (1973) Record Superconductor at 22.3 K. *Physics Today*, **26**, 17. https://doi.org/10.1063/1.3128271

[40] Hirsch, J.E. (2017) Towards an Understanding of Hole Superconductivity. arXiv: 1704.07452v1 [cond-mat.supr-con].

[41] Otto, H.H. (2019) Super-Hydrides of Lanthanum and Yttrium: On Optimal Conditions for Achieving near Room Temperature Superconductivity. *World Journal of Condensed Matter Physics*, **9**, 22-36. https://doi.org/10.4236/wjcmp.2019.91002

[42] Filho, A.I., Lima, P.R.A. and Souza, O.M. (1984) Aspects of Geology of Barreiro Carbonatitic Complex, Araxá, Brazil. In: *Carbonatitic Complexes of Brazil*, CBMM, São Paulo.

[43] Gupta, C.K. and Suri, A.K. (1994) Extractive Metallurgy of Niobium. Taylor and Francis Inc., Abingdon.

[44] Christy, A.G. and Atencio, D. (2013) Clarification of Status of Species in the Pyrochlore Supergroup. *Mineralogical Magazine*, **77**, 13-20.

https://doi.org/10.1180/minmag.2013.077.1.02

[45] Slobinsky, D., Pill, L., Baglietto, G., Grigera, S.A. and Borzi, R.A. (2020) Monopole Matter from Magnetoelastic Coupling in the *Ising pyrochlore*. *Communications Physics*, **4**, Article No. 56. https://doi.org/10.1038/s42005-021-00552-0

[46] Gippius, A.A., Moskvin, A.S., Baenitz, M., Drechsler, S.L., Morozova, E.N. and Otto, H.H. (2003) A Candidate System for Purely Oxygen Antiferromagnetism? *Europhysics Letters*, **63**, 282-288. https://doi.org/10.1209/epl/i2003-00516-1

[47] Borgschulte, A., Rector, J.H., Dam, B., Griessen, R. and Züttel, R. (2005) The Role of Niobium Oxide as a Catalyst for Hydrogen Absorption. *Journal of Catalysis*, **235**, 353-358. https://doi.org/10.1016/j.jcat.2005.08.018

Appendix

Table A1. Coordinates for the fibonacci nets (two-dimensional group *p*6, see also **Figure A1**).

13-subcell net				21-subcell net			
Site	***x***	***y***	***m***	**Site**	***x***	***y***	***m***
1	0	0	1	1	0	0	1
2	4/13	3/13	6	2	1/21	5/21	6
3	5/13	7/13	6	3	2/21	10/21	6
				4	3/21	15/21	6
				5	1/3	2/3	2
Σ*m*			**13**				**21**

m = site multiplicity.

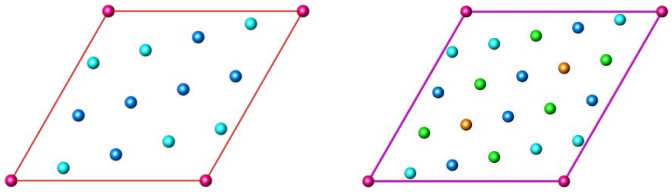

Figure A1. Illustration of the 2*D Fibonacci* nets with differently colored atomic sites (coordinates according to **Table A1**).

Table A2. Comparison between coordinates of the $Nb_{12}WO_{33}$ crystal structure and the Fibonacci net.

Site	**$Nb_{12}WO_{33}$**		**13-Fibonacci Net *)**			
	x	***z***	***x***	***z***	***x***	***z***
W	0	0	0	0	0	0
Nb (1)	0.3663	0.0423	0.38462	0.07692	5/13	1/13
	0.1337	0.9577	0.11538	0.92308	3/26	11/13
Nb (2)	0.2475	0.1358	0.26923	0.15384	7/26	2/13
	0.2525	0.8642	0.23077	0.84616	3/13	11/13
Nb (3)	0.1282	0.2298	0.15385	0.23077	2/13	3/13
	0.3718	0.7702	0.34615	0.76923	9/26	10/13
Nb (4)	0.4165	0.3793	0.42308	0.38462	11/26	5/13
	0.0850	0.6207	0.07692	0.61538	1/13	8/13
Nb (5)	0.2957	0.4715	0.30769	0.46154	4/13	6/13
	0.2043	0.5285	0.19231	0.53846	5/26	7/13
Nb (6)	0.0381	0.2878	0.03846	0.30769	1/26	4/13
	0.4619	0.7122	0.46153	0.76923	6/13	10/13

*) *x* coordinates have been halved in comparison to the original net (see **Figure 7**). The same approach can be applied successfully to the case of $Nb_{16}W_5O_{55}$ using the 21 sub-cell *Fibonacci* net.